Article:
Heeley, A.D., Finney, K.N.N., Szuhánszki, J. et al. (2026) Pilot scale demonstration of potential for decarbonisation of industrial heating processes using hydrogen cofiring. Frontiers in Fuels, 4. 1756561. ISSN: 2813-6217

https://doi.org/10.3389/ffuel.2026.1756561

frontiers in Fuels

TYPE Original Research
PUBLISHED 01 June 2026
DOI 10.3389/ffuel.2026.1756561

OPEN ACCESS

EDITED BY
Hua Meng,
Zhejiang University, China

REVIEWED BY
Eugenio Giacomazzi,
Centro Ricerche Casaccia, Italy
Lorenzo Miserocchi,
University of Pisa, Italy

*CORRESPONDENCE
Andrew D. Heeley,
andy.heeley@sheffield.ac.uk
Karen N. N. Finney,
k.n.finney@sheffield.ac.uk

†These authors share first authorship

RECEIVED 28 November 2025
REVISED 22 January 2026
ACCEPTED 14 April 2026
PUBLISHED 01 June 2026

CITATION
Heeley AD, Finney KNN, Szuhánszki J, Gheit A, Hee JL and Pourkashanian M (2026) Pilot scale demonstration of potential for decarbonisation of industrial heating processes using hydrogen cofiring.
Front. Fuels 4:1756561.
doi: 10.3389/ffuel.2026.1756561

Pilot scale demonstration of potential for decarbonisation of industrial heating processes using hydrogen cofiring

Andrew D. Heeley*†, Karen N. N. Finney*†, János Szuhánszki, Abdulaziz Gheit, Jee Loong Hee and Mohamed Pourkashanian

Energy Innovation Centre, The University of Sheffield Innovation District, Sheffield, United Kingdom

This paper aims to evaluate whether cofiring hydrogen and natural gas mixtures are suitable as industrial furnace fuels and to identify further characteristics that need more detailed understanding to enable successful implementation of fuel switching. The outcome of this research and further investigations will ensure that the full capability of fuel switching becomes available to energy-intensive process operators. Co-firing natural gas and hydrogen leading to dedicated hydrogen combustion are pathways to decarbonise industrial processes and can enable future hydrogen utilisation and interoperability with fossil fuels. The key observations from pilot-scale industrial furnace trials at the University of Sheffield Energy Innovation Centre included: (1) Radiant heat flux depended primarily upon furnace temperature with no relationship measured with varying fuel composition. (2) The chamber geometry, radiant heat flux from solid surfaces and control temperature achieved were more significant to the furnace heat exchange than the fuel mixture. (3) Firing with natural gas and hydrogen mixtures did not affect furnace temperature or uniformity beyond variations attributable to other process conditions. (4) Gas temperatures and species were distributed uniformly within the fully mixed atmosphere, which represented 2/3 of the chamber volume. (5) Gas temperature and species distributions were not affected by fuel composition, therefore measurements from the centre of the chamber were representative of the mean conditions in the fully mixed atmosphere. (6) CFD modelling of the gas and temperature distributions within the furnace enabled thermodynamic and fluid dynamic characteristics to be understood and afforded confidence in experimental and model outcomes. Co-firing hydrogen with natural gas and dedicated hydrogen firing as an interoperable fuel to substitute for natural gas could be a key means to decarbonise hard to abate foundation industries, whilst making continued use of existing capital assets. This investigation demonstrated that understanding hydrogen firing and co-firing will enable the mitigation of perceived risks arising from decarbonisation of energy-intensive industries with low and zero carbon fuels.

KEYWORDS
heat transfer, high temperature furnace, hydrogen, industrial combustion, low-emission combustion technologies, sustainable fuels

1 Introduction

Natural gas firing enables efficient energy usage across a range of industrial settings, particularly for direct-fired, high-temperature processes. However, as a fossil fuel, stringent emissions targets necessary for achieving IPCC commitments cannot be satisfied with continued usage of natural gas as a primary fuel for industrial heating.

The foundation industries, principally: metals, glass, cement, ceramic and minerals manufacturing all require significant capital investment to deploy manufacturing processes and to abate consequent carbon dioxide (CO_2) emissions from high temperature heating equipment (Griffin and Hammond, 2019). The capital equipment installed within these manufacturing industries have long durations of use, typically exceeding 25 years lifetime from installation to decommissioning. The decision to install new technology requires a vision of the future capability required, reliable engineering designs and production forecasts to decide whether the final plant would afford continued business viability, therefore it has a risk attached. Mitigation of the risks around these sorts of investment decisions and demonstration of the cost effectiveness of fuel substitution are essential to the future adoption of net zero carbon processes in manufacturing industries.

Decarbonisation of energy-intensive industrial heating processes through fuel switching and innovation will be necessary to ensure that operations continue to be viable and operable in an emission constrained world. Low and zero carbon fuels are of increasing interest to satisfy the operating requirements, whilst using similar equipment to existing processes. Much remains unknown about replacing natural gas with hydrogen, for example whether process conditions similar to the existing operations will be readily achievable. Hydrogen affords fuel-fired plant operation without incurring IPCC scope 1 CO_2 emissions, however, the potential exists for generating increased oxides of nitrogen (NOx) from thermal sources and other atmospheric pollutants when substituting for hydrocarbon fuels because hydrogen burns with higher flame temperatures (Leicher et al., 2020; Srinivasarao et al., 2024; Schmidt et al., 2023). Understanding the impact of hydrogen upon industrial process heating characteristics is essential to the adoption, operability and viability of decarbonised fuels. The heat transfer between solid surfaces, gas temperature and gas species distributions within the chamber volume, with specific consideration of potential increased thermal NOx emissions from the higher flame temperatures attained with hydrogen firing will all be important considerations, alongside maintaining the process operability (Ilbas et al., 2005; Pan et al., 2023).

The flame characteristics for natural gas and hydrogen firing are reported to also affect convective and radiative heat transfer to processes in small scale experimental equipment (Mayrhofer et al., 2021; Mayrhofer et al., 2022; Okafor et al., 2014; Schimdt et al., 2023; van der Drift et al., 1996). Investigations have been undertaken that address hydrogen firing in specific circumstances or combustion system configurations, such as: micro-burner configurations using premixed combustors for gas turbines (Liu et al., 2023), oxygen-fuel firing using slot type burners (Oh et al., 2015) and small scale equipment, with confined dimensions (Yang et al., 2021; Oh et al., 2013). Further investigations at pilot scale, have focussed upon emissions (Schwartz et al., 2024) and flameless modes of combustion (Lopez-Ruiz et al., 2024). It is essential to therefore understand further the impact of using hydrogen within high temperature manufacturing processes at production scale, using typical industrial burner configurations to enable its adoption within energy-intensive industries. Undertaking pilot scale testing enables the step from laboratory and small-scale firing results and combustion in confined spaces to dimensions that are representative of production plants to be evaluated.

Enabling substitution of natural gas with hydrogen requires that the characteristics of the energy release and heat transfer resulting from combustion that consequently becomes distributed into the process are understood. This will enable suitable adaptations to use the fuels effectively to be determined and ideally will enable their usage within existing process plants. Adaptation of natural gas fired processes to hydrogen fuel requires comparison of combustion characteristics in representative cases at equivalent operating conditions for each fuel. The experimental cases measured within this test programme were representative of typical process conditions encountered in manufacturing, therefore they inform on the usability of hydrogen in manufacturing processes. Translation of outcomes from this project to full scale production plants will need modelling of the full-scale equivalent process and this requires validated models to be determined before application as design tools. We will demonstrate that the pilot-scale experimental work undertaken within this study compared well with computational fluid dynamic (CFD) model predictions of the characteristics of the pilot plant. This will provide confidence that CFD predictions, based upon pilot scale testing could be extrapolated to design full-scale plants with further validation of the model against experimental observations.

Research has demonstrated that the radiation from hydrogen flames is emitted over a different range of frequencies than occurs from fossil fuel flames and can have lower gas emissivity in some regions of the infrared spectrum, depending upon the proportion of combustion products generated (Ceriello et al., 2021; Demuynck et al., 2011; Kounalakis et al., 1991; Shudo and Suzuki, 2002; Zhang et al., 2023). Radiative heat exchange within high temperature chambers is dominated by near and short wavelength infrared frequencies, rather than mid-wave infrared frequencies, in which the major absorption and emission bands for water vapour and carbon dioxide arise (Kounalakis et al., 1991; Rhine and Tucker, 1991). The total radiative heat exchange will be affected by infrared absorption and re-radiation within the gas volume, however the most significant contribution to this exchange in high temperature chambers arises from direct radiation between solid surfaces (Rhine and Tucker, 1991; Zhi et al., 2018). Radiation heat exchange between the solid walls of the chamber and the products (or other solid objects) and gases inside the chamber promotes the development of steady-state conditions and uniform temperature distribution. The radiation, absorption and re-radiation exchange mechanisms lead to the inside surface temperature of the chamber determining the total radiation heat transfer (Rhine and Tucker, 1991).

The radiation heat transfer and gas emissivity values reported and analysed by Ceriello et al., 2021, Demuynck et al., 2011, Kounalakis et al., 1991, Shudo and Suzuki, 2002 and other similar published papers concerning hydrogen combustion were based upon measurements local to the flame region or were

undertaken in equipment having confined dimensions. These investigations have not necessarily included evaluation of all of the energy derived from the fuel in consequence and represent the spectral irradiance, excluding the effects of reradiation between surfaces. The total radiation exchange requires assessment of the total heat transfer between the gases and chamber and between the surfaces (Mayrhofer et al., 2021; Mayrhofer et al., 2022). Radiative heat exchange between solid surfaces confers most of the heat transfer within large-scale and high temperature industrial heating process chambers, owing to the enhancement of emissivity and quartic power of radiant sources, respectively (Rhine and Tucker, 1991). Radiation heat exchange attains near unity relative emissivity in large heating chambers, resulting from the dimensions and that is particularly pertinent for high temperature processes when combined with the consequent high thermal radiance (Rhine and Tucker, 1991; Quinn, 1967; Zhi et al., 2018). The effects of scaling upon the suitability of a chamber geometry to deliver heat into a process uniformly are also important, hence validating CFD modelling of pilot scale equipment with experimental results enables extrapolation of results to larger scale, production plant with increased confidence in the accuracy of prediction (Mayr et al., 2017).

This investigation was based upon measurement and modelling of using a typical industrial diffusion flame burner on a pilot scale heating chamber and considered the hypothesis that the useful heat transfer into the chamber from combusting the same thermal input of fuel would be independent of the ratio of hydrogen and natural gas in the fuel mixture. The caveat applied that the similarity of useful heat release into the chamber should hold true, if other operating parameters that could affect heat exchange remained comparable, for example: excess air, waste gas extraction rate, furnace pressure and chamber exhaust temperature. The energy inputs and outputs for the combustion process and heat exchange with the furnace chamber must balance, therefore any energy that is released and not exchanged by radiation must either be exchanged by convection or exhausted (Mayrhofer et al., 2021). Irrespective of the ratio between different means of transferring the heat released, if the exhaust gas heat flow, heat losses and thermal input from the fuel are the same, then the heat released within the chamber must also be the same.

The total radiant heat flux measured at the chamber walls represents the nett heat exchange between the solid surfaces within view inside the chamber and from the hot gases to these surfaces and represented the heat transfer that contributed the thermal input received by products and surfaces inside the chamber. Measurement of the radiant heat flux incident upon a surface is the most relevant metric to the product heating capability of high temperature industrial furnaces, hence this parameter was chosen to represent the heat exchange in the pilot scale furnace.

Radiant heat in fuel-fired furnaces is derived from the total heat released from combustion and exchanged between the combusting fuel and chamber, therefore the flame shape and characteristics become pertinent to understanding the operation of the process. Hydrogen is expected to combust preferentially compared to natural gas (represented as methane in many experimental and model investigations) when co-firing a fuel mixture comprising these two components. This would lead to high flame temperatures in the combustion region immediately adjacent to the burner quarl and methane combustion being delayed. This would lead to differences in the heat release distributions between dedicated natural gas fuel and co-firing fuel mixtures expected in both experimental measurements and CFD predictions (Srinivasarao et al., 2024; Xu et al., 2021).

The hypotheses posited and explored within the research undertaken and reported within this work were that:

1. The total radiative heat transfer within the chamber does not vary significantly between equivalent cases firing natural gas and hydrogen fuels
2. The gas temperatures and compositions achieved uniform distributions within the fully mixed gas atmosphere, thereby enabling uniform operating conditions to be measured using sparsely distributed sampling positions
3. The experimental characteristics measured could be represented sufficiently well to afford CFD modelling of the pilot scale process and extrapolation to full scale plants would be feasible based upon applying the model to different geometries

2 Experimental methods and materials

The pilot scale furnace at the University of Sheffield, Energy Innovation Centre (EIC) was operated with natural gas and hydrogen firing in different fuel mixtures between 0% and 100% of each component. The characteristics of the gas atmosphere and radiant heat exchange within the chamber were measured using invasive probing and compared with CFD model representations of the chamber thermodynamics and fluid dynamics at different conditions.

2.1 Experimental equipment

The pilot-scale furnace is a 900 mm × 900 mm cross-sectional area x 3632 mm length gas-fired, rectilinear combustion chamber. A schematic diagram of the pilot plant is presented in Figure 1. The internal geometry is defined by the furnace structure and refractory lining mounted on the inside of the metal shell, as represented in Figure 2. The plant has been constructed to satisfy all BS, EN and ISO standards applicable to high temperature, thermo-processing plants. The furnace represents a scaled version of a typical process heating chamber used in manufacturing, including all of the relevant control, monitoring, data recording and automated safety systems.

There are 5 pairs of water-cooled pins (as shown in Figures 1, 2) that present an incrementally variable load to a maximum of 200 kW dissipated to the water-cooling system. The water-cooled load pins were not used in the programme of comparative tests undertaken to enable consistent firing rates to be used for all fuel mixtures up to 100% hydrogen.

The physical dimensions of the test furnace are constrained, having a length to width and height ratio of approximately 4:1. The relative emissivity enhancement arising in large volumes will not be fully developed in this pilot-scale chamber because of the limited dimensions but would have increased compared with the values in open space (Quinn, 1967; Zhi et al., 2018). Furthermore, the

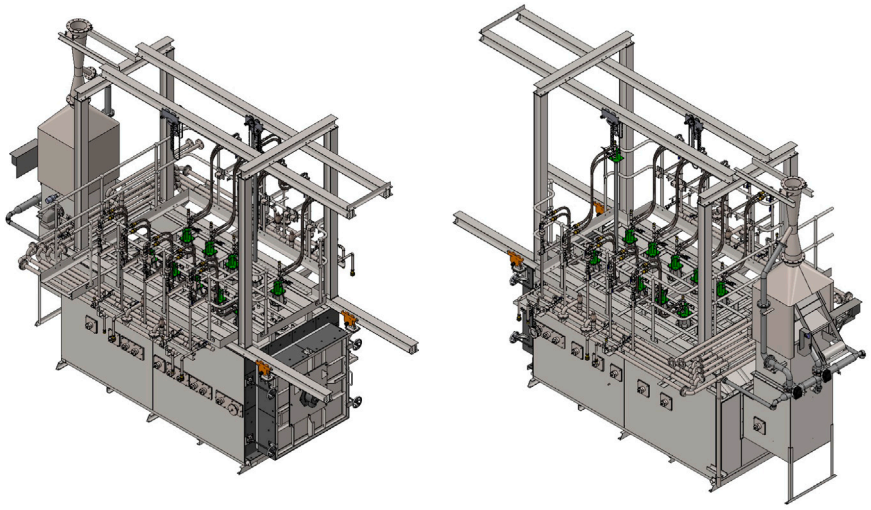

FIGURE 1
Schematic diagram of the pilot scale furnace used for experiments, illustrating water-cooled pins and burner mounting.

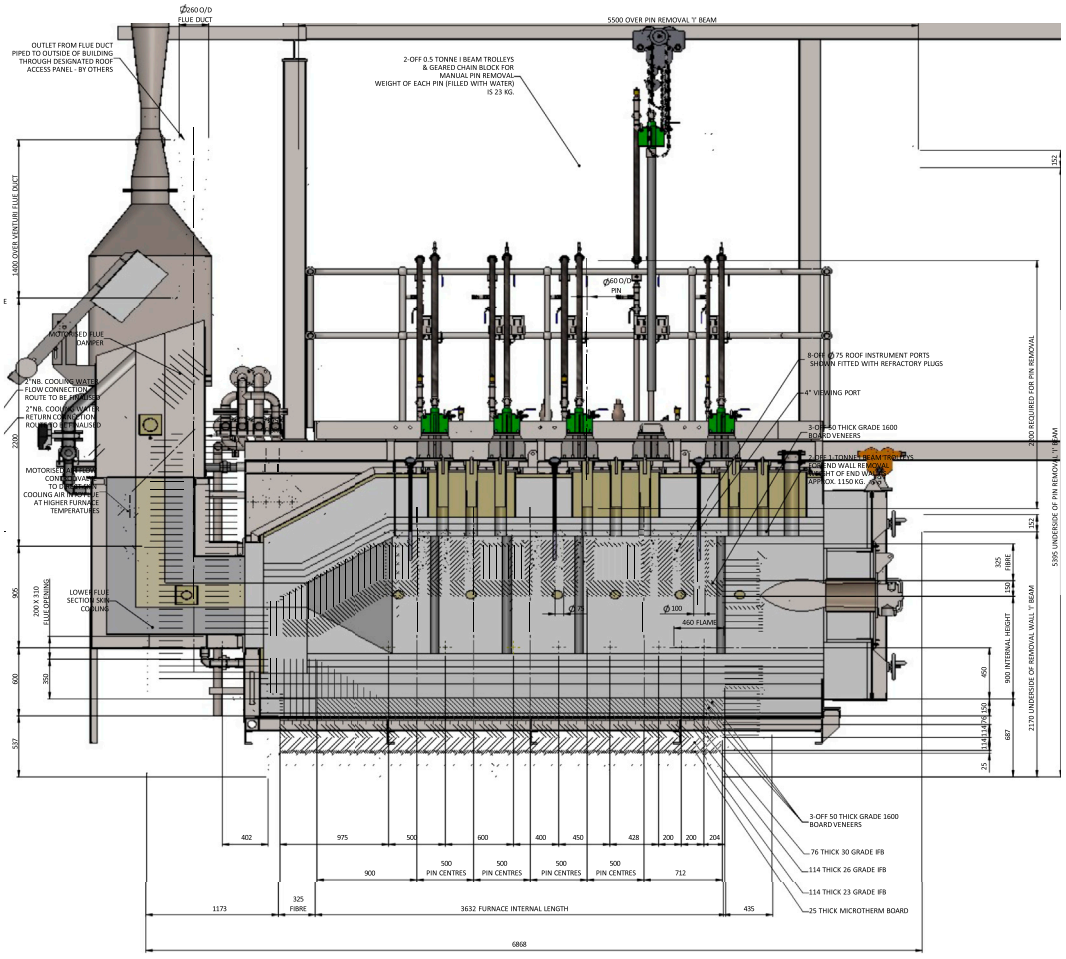

FIGURE 2
Schematic side-view of pilot furnace, illustrating internal cross-section, sample ports and cooling pins.

TABLE 1 Locations of the measurement ports on the EIC industrial hydrogen test furnace; distance is from the front/burner wall to mid-point on the port.

Port	Left hand side (mm)	Right hand side (mm)
1	484	372
2	862	572
3	1,062	1,000
4	1,362	1,450
5	1,562	1,850
6	1,862	2,450
7	2,362	2,950
8	2,562	-
9	2,862	-
10	3,362	-

recirculation of gases in the fully mixed condition, the magnitude of which is dictated by the ingoing combustion product and outgoing exhaust gas volumetric flows, creates a stirred chamber volume that promotes temperature and gas distribution uniformity. The rectilinear shape of the chamber is not ideal for emissivity and temperature uniformity enhancement, for which spherical and cylindrical shaped chambers are known to be better.Rectilinear shaped volumes are known to be sufficiently uniform to afford uniform conditions, in practice, if the ratio of length to width dimensions is sufficiently high, typically achieving good temperature uniformity above 4:1 or 5:1 (Quinn, 1967; Rhine and Tucker, 1991).

As identified in Figure 1, seventeen sample ports are located along the side walls of the furnace. These allow access into the chamber for inserting the measurement probes both within the flame and in the partially and fully mixed regions downstream at various points. Table 1 outlines the distances from the front (burner end) wall at which these measurement ports are positioned, for both sides of the furnace. Depending on the combustion conditions and other operating parameters, Ports 1 and 2 were used for undertaking transects through the flame (so used for in-flame determinations), whilst Port 4 and onwards were typically considered to be in the fully mixed region of the furnace. The probes were inserted through the sidewall sample ports to different measured depths into the chamber to achieve transects, and for full furnace characterisation and mapping, multiple ports were used, where possible.

The fuel was burned using a single, nozzle-mix/diffusion flame Honeywell Kinemax series 3-G gas burner (as seen in Figure 3), that is designed to fire any mixture ratio of hydrogen and natural gas. The burner was mounted centrally in one end wall of the chamber, illustrated in Figure 1 and which projected combustion gases along the chamber length, with extraction achieved through the natural draught exhaust flue that is mounted on the opposite end wall and aligned with the burner centreline, illustrated in Figure 2. The burner fires natural gas and hydrogen as individual fuels and cofires a mixture of the two gases in any proportion up to the nominal 300 kW maximum total thermal input, with stable operation across a range of firing rates to 90:1 turn-down ratio. This capability was not required here, so the usable turn-down ratio was constrained to 10:1 within the control system. The fuel and air mass flow rates were modulated to maintain either thermal input or chamber temperature set point and could be set to achieve constant flow rates independently. The air:fuel ratio can be set to achieve any free oxygen concentration in the exhaust above 0.5 vol% (dry). Oxygen concentration can either be controlled to a given value, based upon the excess air set point or allowed to settle at a nominal condition, based upon the flow rates of air and fuel. Irrespective of how the free oxygen concentration is derived, the fully mixed atmosphere measured within the exhaust gas always has to exceed this lower limit to maintain fuel supply to the burner, otherwise an automated plant safety shutdown is initiated. The lower limit of the excess air requirement to achieve this oxygen concentration also ensured complete combustion, with low carbon monoxide concentrations in the fully mixed combustion product gases.

Natural gas can be supplied up to approximately 30 m^3/h (STP) equivalent to 305 kW nett thermal input from the site distribution pipeline and supplied to the burner at 100 mbar(g) via the gas mixing and control skid. Hydrogen can be supplied by EIC generation and storage facilities with a maximum flow rate of 106.5 m^3/h (STP) equivalent to 320 kW nett thermal input. The hydrogen is supplied at 30 bar(g) which is reduced in stages to 100 mbar(g) supply pressure to the burner by a series of pressure regulators on the gas mixing and control skid The burner and internal geometry of the chamber are illustrated in Figures 3a,b, respectively.

The pilot furnace was fired with natural gas and hydrogen at equivalent thermal inputs of nominally 75 kW and air:fuel ratio set points to achieve 10% excess air above the stoichiometric combustion requirement. The stoichiometry varied with the cofired fuel mixtures, according to calculations based upon the air:fuel ratio requirement of each species contained within the fuel, weighted according to the fuel composition. The chamber volume attained a steady-state temperature of approximately 850–900 °C with natural gas firing at nominal 75 kW and approximately 800–850 °C with hydrogen firing and no thermal load in the chamber because of the increased excess air described in section. This lower firing rate testing without the thermal load, whilst maintaining moderate operating temperatures up to 900 °C, enabled direct comparison of operation with different fuels at similar process conditions. These temperatures were representative of typical moderate to high temperature conditions encountered in industrial heating processes, such as curing ovens and heat treatment furnaces.

2.2 Experimental measurements

Measurements were acquired using invasive probes inserted into the chamber through the sample ports along each sidewall. The radiant heat flux (RHF) around the furnace chamber sidewalls and gas temperature and species distributions through the chamber volume were measured for 100% natural gas, 100% hydrogen and co-firing different ratios of natural gas to hydrogen. The measurements were compared at the steady-state conditions achieved for each case to provide comparison of operating conditions. The gas temperature and species probes were inserted to different depths across the chamber to map these distributions co-

FIGURE 3
(a) End elevation of burner illustrating central gas inlet ports and peripheral, angled air inlet ports that introduce fluid swirl and **(b)** end elevation of pilot furnace chamber geometry (shown from the burner end), illustrating control and monitoring thermocouples, sample ports and refractory lining components.

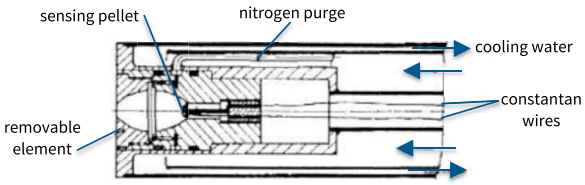

FIGURE 4
Schematic diagram of measuring tip of IFRF design ellipsoidal radiometer probe.

planar with the burner centreline and the radiant heat flux probe was positioned to align coplanar with the ports in the sidewall surfaces, thereby mapping the longitudinal distribution of thermal irradiance received by these refractory surfaces.

2.2.1 Radiant heat flux measurements

Radiative heat flux incident upon the furnace walls was measured using an International Flame Research Foundation (IFRF) design ellipsoidal radiometer. The core of the radiometer is the water-cooled ellipsoidal cavity with an orifice on the focus side and a thermopile sensing the total heat delivered at the receiver, illustrated in Figure 4. Radiation entering through the orifice at almost any angle of incidence within the hemisphere is reflected onto the sensing element of the thermopile, owing to the ellipsoidal geometry of the cavity. The cavity is covered with a gold film, having high reflectivity to minimize radiation losses arising from absorption by the surface. The thermopile produces an electromotive force that is proportional to the amount of radiant energy absorbed by its sensing element. The ellipsoidal cavity is divided into two parts by a Zinc Selenide (ZnSe) window, which has uniform, high transmissivity over the range of radiation wavelengths from 0.6 μm to 14 μm, thereby affording capture of radiation from the orange-red visible to the long-wave infrared regions of the spectrum. The inner section of the cavity is isolated from the external environment to avoid any contamination from the gases within the combustion chamber. The outer part of the cavity is purged with a nitrogen flow to reduce the infiltration of contaminants from the chamber and avoid deposition of soot/particles/impinging gas on the inner window and reflective surface of the cavity.

2.2.2 Gas temperature measurements

The gas temperature distribution inside the furnace chamber was measured using a water-cooled IFRF design suction pyrometer. A schematic diagram of the probe is presented in Figure 5. The platinum-rhodium alloy thermocouple (designated as type B) is protected from chemical attack by a sintered alumina tube. This is surrounded by two concentric radiation shields that mitigate the effect of incident radiation from the chamber surfaces on the thermocouple junction. The gases are drawn through the outer and inner shields and the alumina protection tube to pass over the thermocouple at high velocity (70–150 m/s) so that the temperature of the thermocouple and gases attain equilibrium. This obviates the need for correction factors to account for the radiative heat losses to and heating from the solid surfaces. Sample suction was delivered through a compressed air venturi ejector, supplied at 3 bar(g) pressure from the instrument air supply.

The measuring junction at the probe tip was inserted through the sidewall ports to different depths into the chamber volume, the data recorded representing a position versus temperature map that was interpolated to define the temperature distribution across the chamber volume at the planar midpoint.

2.2.3 Gas composition measurements

A bespoke water-cooled, gas sampling probe was constructed to enable the gaseous products of combustion to be extracted for analysis from inside the chamber, including the flame region adjacent to the burner quarl. The probe was inserted through the sidewall sample ports to different, measured depths into the furnace chamber that enabled measurements from several points across the width from each port. This measurement technique enabled the distribution of gas species to be mapped similarly to the gas

temperature. The sample gas extracted was analysed using Fourier Transform Infrared (FTIR) spectroscopy that enabled rapid and continuous measurement of the concentrations of various gas species present in the combustion atmosphere. The uncertainty around the FTIR measurements was estimated to vary from 2.5% of the measured value for the oxygen, water vapour and carbon monoxide concentrations to approximately 10% of the measured value for NOx and carbon dioxide values. Residual hydrogen concentration was measured using a micro gas chromatograph (micro-GC) within the flame region and fully mixed atmosphere.

Ports 1 and 2 on the chamber sidewall (at 372 mm and 572 mm from the burner end wall) enabled measurements of gas samples from within the flame around the furnace chamber centreline, indicating the lateral extent of the flame envelope. Measurements from a single position on the chamber lateral centreline at 1,450 mm along the chamber enabled comparative measurements of the fully mixed combustion product species. Samples from beyond 1,000 mm along the length of the chamber enabled measurement of the fully mixed combustion product gases that represented the composition within most of the chamber, as far as 2,950 mm from the burner end wall. The samples from Port 10 (the final longitudinal position available) afforded measurement of the exhaust gases immediately adjacent to the flue.

The gas distribution, based upon these series of point samples, enabled the extent of the flame envelope and the distribution of fully mixed combustion products to be determined from the presence of indicator species. The flame envelope is identified by the transition between the presence of unburnt fuels (methane CH_4 and hydrogen H_2) and partial combustion products (carbon monoxide CO for hydrocarbon fuels) to the principal products of complete combustion (carbon dioxide CO_2, NOx, and water vapour H_2O).

2.3 CFD modelling

A CFD model was constructed during the furnace design process using ANSYS Fluent simulation software to represent the fluid dynamics under the conditions tested in this programme, including both combustion and subsequent dispersion of the gas products through the chamber volume. The model was used to study how comburent gases mix and combust within the flame region and how the combustion products interact with the chamber and surrounding quiescent atmosphere. The following models were used: the k–ω SST turbulence model for fluid motion; a species-transport model coupled with the Eddy-Dissipation reaction model for fuel-oxidant chemistry; and the P1 model for radiation. Heat transfer through the wall was represented by a 1-D conduction model using prescribed wall material properties, without explicitly meshing the solid domain. Residuals for all transport equations (momentum, continuity, energy, radiation, species) reached the order of magnitude 1×10^{-6} or better, and temperature and velocity variables at several locations were inspected to confirm a converged solution. The mesh comprised 5.2 million cells (a mix of hexahedral and tetrahedral elements) and was validated by a mesh-independence study, with refinement concentrated in regions of high solution gradient (flame and mixing zones). A sample snapshot of the CFD domain is shown in Figure 6 outlining the location of the burner, chamber volume, walls and the outlet. The model reproduced fluid-dynamic features observed experimentally and enabled evaluation of gas-species uniformity, gas temperatures and chamber heat transfer.

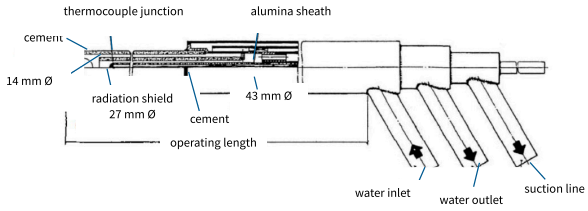

FIGURE 5
Schematic diagram of IFRF suction pyrometer and radiation shield configuration.

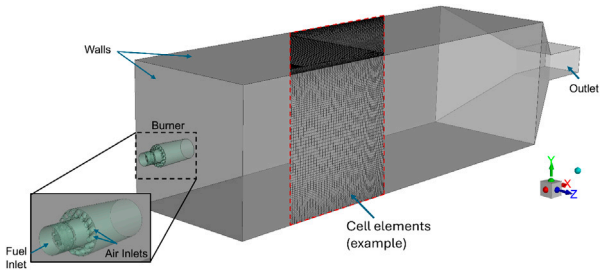

FIGURE 6
Schematic diagram of the CFD model domain of the burner and chamber.

3 Experimental cases for comparisons

The furnace was fired using dedicated natural gas, dedicated hydrogen and co-firing natural gas with hydrogen at several different compositions for similar firing rates and air to fuel ratio set points, as outlined in Table 2. The thermal firing rate has been evaluated based upon the flow rates and tabulated fuel properties (Rose and Cooper, 1977). The furnace was fired with natural gas to provide baseline gas temperature, gas species and radiant heat flux data for comparison with the test cases when firing and co-firing hydrogen.

The air and fuel flow rates used in the test cases represent the mean values of the parameters measured and have been affected by the flow control actuator characteristics and particularly the limitations around minimum flow rates achievable and variability with controller demand. Further measurements across a range of firing rates, operating temperatures and fuel mixtures were acquired and are used sparingly in this analysis owing to experimental uncertainties affecting the process operation data.

Additional conditions at different firing rates of 70 kW, 80 kW and 90 kW with 100% hydrogen were tested to evaluate the magnitude of effect that firing rate variations would have upon furnace conditions compared with the change of fuel composition.

The CFD cases modelled represented similar conditions to the experimental observations and included: dedicated natural gas and

TABLE 2 Fuel and air flow rates achieved during the test programme for natural gas and hydrogen fuel firing comparison at steady-state, nominal thermal inputs of approximately 75 kW and 135 kW.

Fuel mixture	NG fuel flow m^3/h	H_2 fuel flow m^3/h	Air flow m^3/h	Total exhaust flow m^3/h	Aim exhaust oxygen % dry	Approximate firing rate kW
100% natural gas	7.4	0.0	78.8	86.2	2.0	75.4
70% NG/30% H_2	5.2	8.9	74.9	89.0	1.0	79.7
60% NG/40% H_2	4.4	10.2	73.6	88.2	2.1	75.4
50% NG/50% H_2	3.6	12.2	72.1	87.9	2.7	73.3
40% NG/60% H_2	3.0	14.4	69.5	86.9	2.1	73.8
30% NG/70% H_2	2.3	18.9	69.5	90.7	0.8	80.1
25% NG/75% H_2	1.5	23.0	68.0	92.5	-	84.3
100% H_2	0.0	24.3	65.6	89.9	2.1	72.9

hydrogen firing and co-firing mixtures of the fuels to achieve the thermal input and air to fuel ratio set points and additional excess air characteristics that were representative of the conditions measured. The changes in the flame region, extent of combusting gases and the outcomes for the fully mixed gas temperature distributions were compared between these representative cases and compared to the experimental samples to confirm the similarity of gas and temperature distributions. The CFD model predictions were then interpreted to provide a more detailed understanding of the combustion product characteristics measured in the experimental investigation.

4 Experimental and CFD modelling results

Example images of the flame observed inside the furnace chamber and adjacent to the burner quarl, are presented in Figures 7a,b, illustrating 100% hydrogen firing and cofiring 70% hydrogen with 30% natural gas, respectively. These images were captured through the optical instrumentation/viewing port window mounted on the furnace sidewall, with the centre positioned at 172 mm along the length from the burner end wall. The darker central region in the images was the 'blind' end viewing port mounted on the opposite sidewall of the furnace chamber that provided a closed port and background stop for optical instrumentation.

The visible flames in both cases were optically thin in the visible spectrum, as evidenced by the near transparent images and would be expected for co-firing hydrogen or dedicated hydrogen firing and particularly for diffusion flames firing into an elevated temperature chamber with high background radiant intensity compared to the gas.

The different flame intensity observed in these images did not illustrate the differences between the infrared radiant emissions from fuel mixtures, which are affected significantly by the differences in CO_2 and H_2O concentrations in the combustion product gases. CO_2 has higher optical thickness than H_2O and these molecules radiate and absorb within different infrared frequency bands, as reported in literature concerning heat exchange in furnace chambers (e.g. Khan et al., 1997; Leckner, 1972; Smith et al., 1982). The direct radiation from the flame will be reduced, however the radiative heat exchange in high temperature furnaces is dominated by the total radiation between solid surfaces. The reduction of direct flame radiance does not reduce the heat transfer significantly (Rhine and Tucker, 1991; Tucker and Ward, 2012).

4.1 Radiative heat flux

The radiant heat flux measurements conducted across a range of fuel mixtures between 45% hydrogen co-firing and dedicated natural gas firing, demonstrated that similar heat transfer occurred for consistent furnace temperatures, as illustrated in Figure 8 for 900 °C and 950 °C. Similarly, the relationship between furnace temperature and radiant heat flux measured for a range of hydrogen and natural gas co-firing ratios between dedicated natural gas and 80% hydrogen/20% natural gas but varied process conditions (burner firing rate, furnace temperature, constant thermal input and temperature control mode) is presented in Figure 9.

The radiant heat flux distributions measured along the furnace chamber sidewalls when firing the furnace with dedicated natural gas and hydrogen fuels are presented in Figure 10. The comparison demonstrated that the fuels were interoperable from the perspective of radiation heat exchange into and from the solid surfaces. The consistency of radiant heat flux measured for given furnace temperature, irrespective of the fuel mixture, indicated that hydrogen cofiring and dedicated hydrogen firing provided the same magnitude of heat transfer as natural gas firing to the pilot chamber.

The measurements demonstrated that the total radiant heat flux, therefore heat transfer attributable to radiation exchange, was not affected by the fuel composition. The principal factor that affected radiant heat flux was the furnace temperature achieved, with a correlation factor between 90% and 97% for individual sets of data. The correlation moments were evaluated between radiant heat flux and furnace temperature and hydrogen fraction in the fuel across the range of operating conditions tested (firing rate, furnace temperature, hydrogen to natural gas ratio in the fuel mixture, air flow rate) and port position used to measure the parameter. The correlation moments evaluated between furnace temperature and

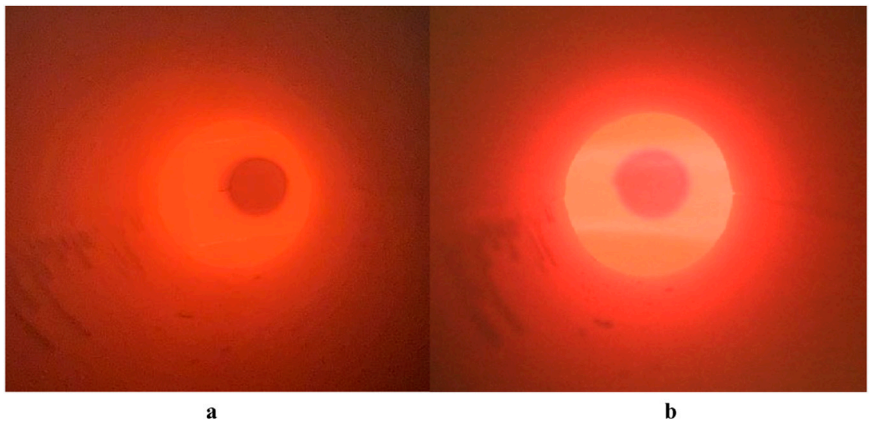

FIGURE 7
(a) Image of 100% hydrogen firing into hot chamber conditions, illustrating a barely visible flame envelope adjacent to the viewing port. **(b)** Image of 30% natural gas – 70% hydrogen mixture firing into hot chamber, illustrating marginally more visible but still optically thin flame envelope adjacent to the viewing port.

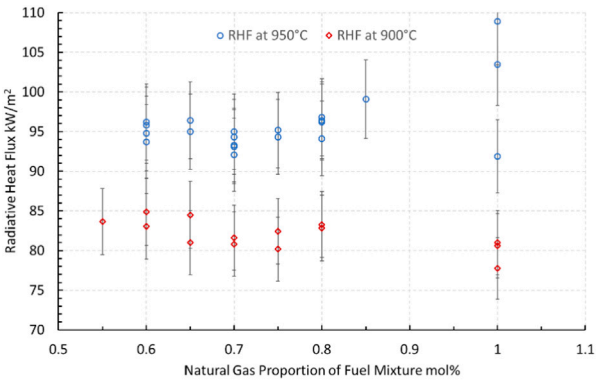

FIGURE 8
Radiant heat flux measured at different hydrogen and natural gas mixture ratios for two example furnace temperatures of 950 °C and 900 °C.

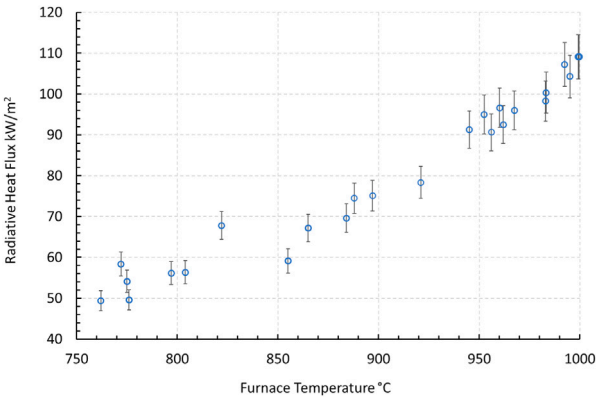

FIGURE 9
Radiant heat flux measured at different furnace temperatures, dictated by process conditions, and hydrogen-natural gas mixture ratios between 0% hydrogen and 80% hydrogen.

radiant heat flux demonstrated that a relationship existed, whereas the correlation moments between hydrogen fraction and radiant heat flux demonstrated no discernible relationship. This demonstrated that there was a definitive relationship between furnace temperature and radiant heat flux that reinforces furnace temperature as the principal determinant of total radiant heat exchange. This aligns with the expectation from large-scale furnace chambers having enhanced relative emissivity that affects radiant heat exchange between solid surfaces, affording equalisation of temperatures between surfaces and approximating blackbody conditions, as confirmed in literature and operational experience (e.g. Rhine and Tucker, 1991; Quinn, 1967).

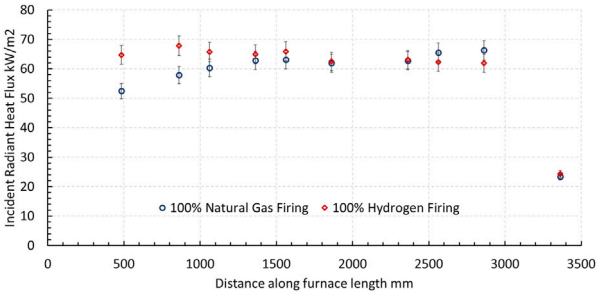

FIGURE 10
Comparison of radiant heat flux measured along pilot furnace chamber for dedicated natural gas and hydrogen firing.

4.2 Gas temperature distribution

The gas temperature transects through the combustion region demonstrated that the highest flame temperature occurred on or near to the burner centreline and that the temperature magnitude increased with the proportion of hydrogen in the fuel mixture, as illustrated by Figure 11a. The gas temperature distributions measured across the furnace width for the fully mixed

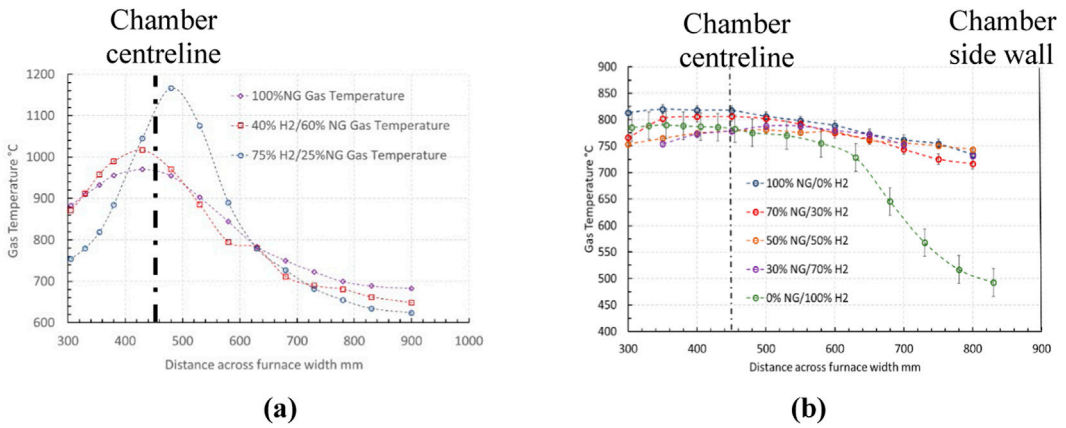

FIGURE 11
(a) Example gas temperature transects at 572 mm from the burner end wall (port 2), illustrating the higher centreline temperatures achieved with increasing hydrogen content of the fuel and **(b)** gas temperature variation for the fully mixed combustion product gases at 1450 mm from the burner end wall at approximately 75 kW firing rate.

combustion products were measured at 1450 mm from the burner end wall (right hand sidewall Port 4) onwards, when firing dedicated hydrogen and co-firing with natural gas. These transects demonstrated that the fully mixed atmosphere achieved uniform gas temperature distribution across at least 60% of the chamber width, with only the boundary region near the sidewalls demonstrating differences. This also enabled further measurements of the quiescent gas to be undertaken from a single centreline position.at 1,450 mm along the chamber from the burner end wall. Typical temperature profiles across the fully mixed region of the chamber at different natural gas - hydrogen fuel gas compositions are presented in Figure 11b.

The gas temperature measurements from natural gas, hydrogen and co-firing of the chamber demonstrated that uniform temperature distribution was achieved within the fully mixed gases at steady state operating conditions across the central 600 mm width of the chamber, irrespective of the fuel mixture. The effect of the sidewall heat losses lowered the gas temperature measured locally but most of the chamber achieved uniformity within 10% of the mean temperature measured by both the control thermocouple, that represented the chamber temperature and suction pyrometer, that represented gas temperature.

Mean gas temperature measurements for the fully mixed atmosphere at 1,450 mm from the burner end wall and measured on the burner centreline for different fuel compositions are presented in Figure 12.

The temperatures measured by the furnace control thermocouple and suction pyrometer for the fully mixed gases were demonstrably independent of the natural gas to hydrogen ratio in the fuel mixture. The mean furnace temperature measured by the control thermocouple and the mean gas temperature measured by the suction pyrometer achieved Pearson correlation coefficients between 98.5% and 99.5%. These measurements demonstrated a definitive relationship between the furnace and gas temperatures across the range of fuel compositions tested and no correlation with the proportion of hydrogen in the fuel mixture. The variation of furnace temperature and gas temperature measured

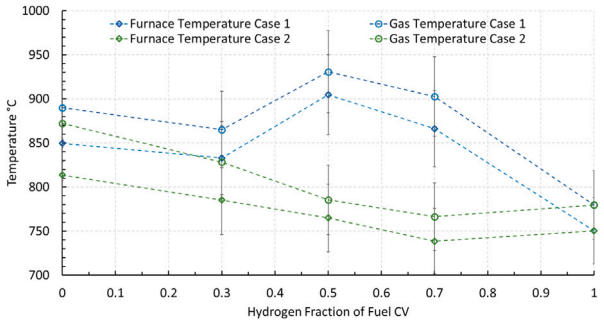

FIGURE 12
Variation of furnace control thermocouple temperature and centreline gas temperature of fully mixed atmosphere with proportion of hydrogen in fuel mixture.

with changing fuel mixture resulted from differences in the operating conditions between cases tested at different times. It was evident that the extent to which the refractory materials had achieved thermal equilibrium affected the temperature measured but was unknown between test days. Similarly, variability of the air to fuel ratio within the control system and purge air that introduced additional excess air into the combustion products caused cooling of the chamber temperature observed in these measurements. These undefined parameters caused variability in the test conditions and increased the uncertainty compared to the magnitude estimated from the measured data. The non-linear response of actuators to changes in firing rate, air and fuel flow rates and control temperature are typical of heating processes in manufacturing. The measurements acquired from the pilot scale investigations undertaken are therefore considered representative of the typical behaviour of full-scale manufacturing equipment.

The heat transfer to the solid surfaces may be affected by the different stirred conditions with varying fuel composition, with the evidence that the 100% hydrogen firing case had lower temperatures

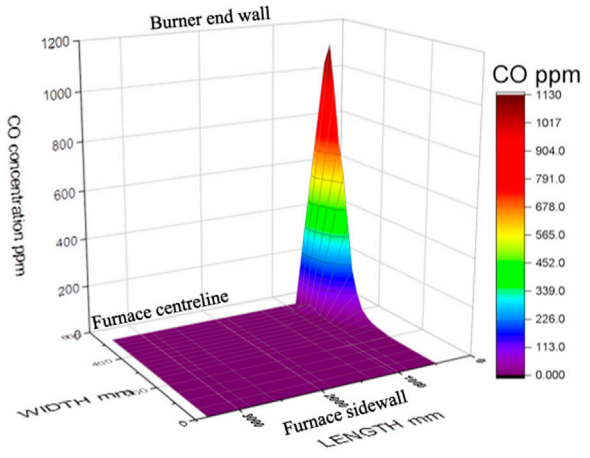

FIGURE 13
CO distribution along and across the pilot furnace, demonstrating the extent of the combusting gases, that is, flame extent for dedicated natural gas firing.

towards the wall (as shown in Figure 11b), however, this would need confirmation by further investigation and analysis.

4.3 Gas species distribution

Gas species were also measured within the furnace, using the invasive sampling probe delivering a sample to the FTIR gas analyser, either directly through a sample line and water drop-out or via a diluter, when sampling from the in-flame region. CO concentrations measured across and along the chamber in transects are mapped in Figure 13 for dedicated natural gas firing. This outlines the peak immediately adjacent to the burner (as assessed at 372 mm and 572 mm from the burner end wall), through the minimal levels seen in the fully mixed gas volume (Ports 3 through 6) and to those recorded adjacent to the exhaust flue (Port 10).

This CO distribution indicated the extent of the combusting gases projected from the burner position, that is, the end wall at 0 mm along the furnace length and centred at 450 mm across the width. Combustion had completed such that no CO concentration was measured beyond 1000 mm along the furnace length and the flame envelope extended less than 250 mm radius around the burner centreline. The composition measured beyond these limits demonstrated uniformity and zero CO measurements throughout the chamber, indicative of fully combusted fuel and fully mixed combustion product gases.

Observation of the evolution of CO_2 and O_2 provided similar definition of the combusting gas envelope as extending to approximately 200 mm radius around the chamber centreline and between 572 mm and 862 mm along the furnace length from the burner end wall. The CO_2 concentration measured in the fully mixed combustion gases attained 7.6% (dry) with dedicated natural gas firing. The oxygen concentration here was higher than expected, having been set to achieve nominal 10% excess air flow, that is approximately 2.0% excess oxygen in the exhaust when firing natural gas, hydrogen or co-firing mixtures of the two fuels. The exhaust oxygen concentration measured would be equivalent to supplying 36% excess air in the combustion air flow, an equivalent air:fuel ratio of 13.3:1 and providing 23.5% more total air volume than the excess air set point required.

Typical gas species distributions measured across the furnace chamber width from Port 1 adjacent to the burner quarl (at 372 mm from the burner end wall), for different co-firing fuel compositions are presented in Figures 14a–c The lateral centreline position of the furnace and burner (located at 450 mm across the furnace width from the sidewall inner surface) is indicated by the dashed and dotted centreline markers on these figures. These measurements demonstrate that the peak of partial combustion products occurred adjacent to the lateral centreline of the chamber for natural gas and lower proportions of hydrogen in the fuel mixture.

It was evident that the apparent peak of partial combustion products and unburned gases, which was inferred to be the centre of the flame occurred around the burner and furnace lateral centreline when firing with 100% natural gas and up to 40% of the thermal input provided by hydrogen, as illustrated in Figures 14a,b. The measurements with 60% of the fuel thermal input provided by hydrogen, however, revealed that the peak partial combustion products occurred eccentrically to the longitudinal axis, as evidenced by Figure 14c.

The concentration of hydrogen measured within the flame region for 60% and 40% hydrogen co-firing, represented by samples from Ports 1 and 2 at 372 mm and 572 mm from the burner end wall are presented in Figure 15. The hydrogen had been consumed completely within the early stage of combustion and had been consumed prior to the first measurement position when co-firing with 40% hydrogen. These measurements contrasted with the methane and carbon monoxide measurements which demonstrated presence of unburned fuel at 572 mm from the burner end wall (Port 2), illustrated in Figures 14a–c.

The gas species transects through the flame indicated that the hydrogen component of the fuel would be consumed preferentially compared to the natural gas components when co-firing a fuel mixture. Preferential combustion of hydrogen would be expected from its higher diffusivity, flame speed and lower ignition energy, compared to methane.

These preliminary findings concerning preferential hydrogen consumption and effects of geometry and fluid dynamics upon flame asymmetry would need verification by further experimental measurement and modelling across a wider range of conditions.

The minimum oxygen concentration measured on the burner centreline whilst co-firing hydrogen with natural gas was 8% (dry), whereas the combustion air supplied would be capable of sustaining approximately 2% excess oxygen (dry). The high excess oxygen concentration measured indicated that there was significantly more air within the chamber than the control system supplied for combustion.

The gas species sampled across the fully mixed atmosphere when firing 100% hydrogen into the chamber demonstrated higher excess oxygen, achieving a minimum of approximately 13% (dry) on the burner centreline and 17% in the fully mixed atmosphere for the same excess air set point. These measurements indicated that additional air was present in the atmosphere when firing increasing proportions of hydrogen, which resulted from the fixed volume of cooling/purging air being entrained into the combustion region.

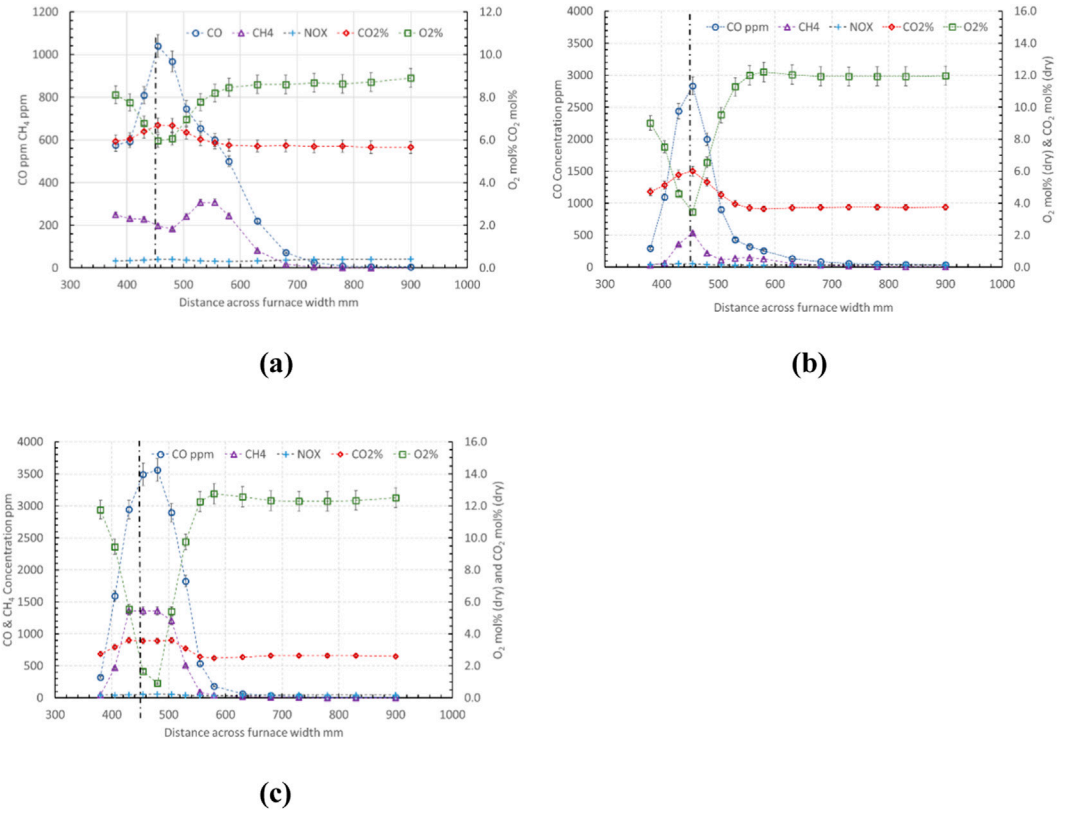

FIGURE 14
(a) Gas species distribution through the flame region when firing natural gas, **(b)** Gas species distribution through the flame region when cofiring 40% hydrogen and 60% natural gas by thermal input and **(c)** Gas species distribution through the flame region when cofiring 60% hydrogen and 40% natural gas by thermal input.

The concentrations of CO and CO_2 in the atmosphere reduced to zero with 100% hydrogen firing, whereas mean NOx concentrations were approximately doubled compared to natural gas firing and co-firing cases. These changes would be expected from the elimination of carbon from the fuel and the higher (peak) flame temperature achieved, as presented in Figure 11a. Correction of NOx concentrations to 3% (dry basis) excess oxygen conditions, would have elevated the specific NOx concentration estimated for dedicated hydrogen combustion by approximately 20% compared to emissions evaluated on mass basis and would have presented invalid data.

4.4 CFD model comparator outcomes

Example temperature distribution predictions from CFD modelling cases of this pilot furnace firing 100% natural gas, 100% hydrogen and 50:50 co-firing cases are presented in Figures 16a–c. These figures illustrate the gas temperatures of the burner jet expanding into the quiescent atmosphere for these different firing conditions and the development of the fully mixed chamber atmosphere. The significantly lower chamber temperatures and differences in flame shape for the cofiring case were probably due to the differences in excess air.

The combustion region shape varied between the natural gas and hydrogen firing cases, demonstrating different penetrations of the combustion jet into the chamber, evidently arising from increased containment of the hydrogen by the ingoing air.

Asymmetry of the gas temperature and ingoing jet was evident around the combustion region when co-firing natural gas and hydrogen, depicted in Figure 23c as a downward offset of the high temperatures associated with the combustion region.

Local vector plots of the combusting gases at 200 mm into the chamber from the burner quarl are presented in Figures 16a,b, illustrating the fluid flow field locally to the combustion region immediately adjacent to the quarl and demonstrating the effect of the air swirl and gas nozzle flow patterns imposed onto the flame, generating rotational momentum and entraining the gas atmosphere from the surrounding volume.

The combustion region was demonstrated to entrain the recirculating gas atmosphere through the boundary region, locally to the burner in the combustion region, where the atmosphere gases mixed with the combusting gases. This entrainment causes dilution of the flame with combustion products, thereby reducing the gas temperatures and diluting the comburent composition with the recirculated gases. This entrained gas flow also mixes any ingress air captured within the gas stream into the combusting mixture.

The effects of entrainment and combustion, causing expansion of the jet flow into the chamber are illustrated by Figures 18a,b, in which respectively, the predictions for the fluid flow fields at

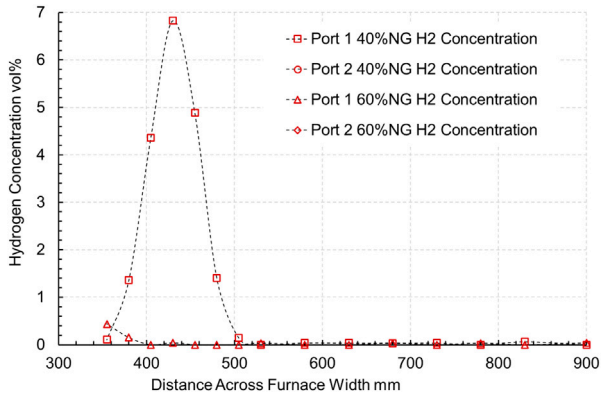

FIGURE 15
Hydrogen concentration in the flame region measured when co-firing 40% and 60% hydrogen fuel composition.

different distances along the chamber length are presented for dedicated natural gas firing and dedicated hydrogen firing.

Similarly to the gas temperature and local flow field vector plots, these CFD model outcomes predicted both increased confinement of the jet with dedicated hydrogen firing and the development of asymmetry in the combustion region gas flows when co-firing natural gas and hydrogen.

There was evidence of the effects of the air swirl from the ports creating a turbulent flow distribution imposing rotation of the ingoing gas onto the jet and that may be expected to be transient.

The experimentally measured positions of peak gas temperatures and the gas temperatures and flow fields observable in the model predictions demonstrated similar asymmetry of the combustion region.

There was evidence from the flow field modelling to support the hypothesis that the burner geometry and interactions within the chamber led to the flame asymmetries and offset peak temperatures measured, particularly the presence of swirl causing turbulence in the gas flow. Further and more extensive experimental measurement and CFD modelling is required to validate the causes of flame asymmetry proposed.

5 Discussion and implications of findings

5.1 Total radiative heat flux and radiant heat exchange

Radiative heat flux was demonstrated to be uniform throughout 60% or more of the chamber, only varying adjacent to the burner and exhaust flue. The total radiation heat flux did not vary with fuel composition, achieving steady-state heat exchange for similar operating conditions but had a definitive relationship with furnace chamber temperature. The operating conditions for example: additional air entrained into the combustion region and burner thermal input rate affected the furnace temperature, therefore, an indirect effect of varying fuel composition was observed via changing proportion of excess air in the combustion product gases.

The water vapour absorption/emission frequency bands being 'optically thin', with transmittance of typically circa 90%, had less effect upon gas radiation than the carbon dioxide absorption/emission bands which are 'optically thicker', with transmittance of typically circa 30%, as described within the introduction. The increased concentration of water vapour arising from hydrogen combustion, achieving up to approximately 30 vol% for dedicated hydrogen firing in air compared to approximately 18 vol% for natural gas combustion would therefore have less effect upon radiation passing through the gas volume than the corresponding reduction of the CO_2 concentration. Combustion with increased proportions of hydrogen in the fuel mixture would lead to reduced absorption and re-radiation from the gas volume, however this may not be obvious in high temperature chambers, such as used in this investigation and more widely in industry because of the dominance of radiation between solid surfaces. The combustion product gases approximate 'grey' gas radiation conditions, for which the absorbed and emitted radiant energies attain equilibrium, therefore the gas radiation emissivity and absorptivity become unrelated to the nett heat exchange between surfaces within the chamber, as described in Rhine and Tucker (1991) and Zhi et al. (2018). This further eliminates the effects of gas composition from the ability of a high temperature chamber to deliver process or product heating.

The geometry of the chamber used for this investigation, having approximately a 4:1 length to width ratio, afforded enhanced relative emissivity of the chamber walls, roof and hearth by reflecting radiation between the enclosure surfaces. The heat transfer within the chamber approaches blackbody conditions with increasing length to width ratio, irrespective of the material emissivity values in free space, as reported by Zhi et al. (2018), Rhine and Tucker (1991) and others, thereby ensuring uniform temperature distribution. The principle that large dimension chambers attained enhanced emissivity is known to extend to cubic geometries as well as cylindrical tube and spherical furnaces for which Quinn (1967) originally developed the theory. In practice, provided that the geometry afforded suitable length to width ratio. The pilot furnace was relatively short but had sufficient length to width ratio to afford enhanced emissivity of the solid surfaces, even if blackbody conditions were not expected to be achieved fully.

Additionally, the recirculation of the fully mixed combustion gases, which represented approximately 30 volume changes of gas per hour within the chamber, promoted the attainment of uniform temperature distribution in the rectilinear chamber. The chamber had sufficiently large dimensions to afford the gas to expand unconstrained and recirculate throughout the volume to enable development of uniform gas temperature and species distributions from entrainment of quiescent combustion atmosphere gases into the burner jet (Forstall and Shapiro, 1950). The ideal furnace shape to promote gas recirculation and temperature uniformity is spherical, then cylindrical geometry and rectilinear geometry being the least suitable. Many production furnaces have features intended to promote recirculation of gases and enhancement of temperature uniformity, such as target walls that force gas flow direction changes to enhance recirculation, however even rectilinear shaped chambers can achieve uniformity if sufficient gas recirculation occurs, and the dimensions are sufficient to promote radiation heat transfer (Mayr et al., 2017). The

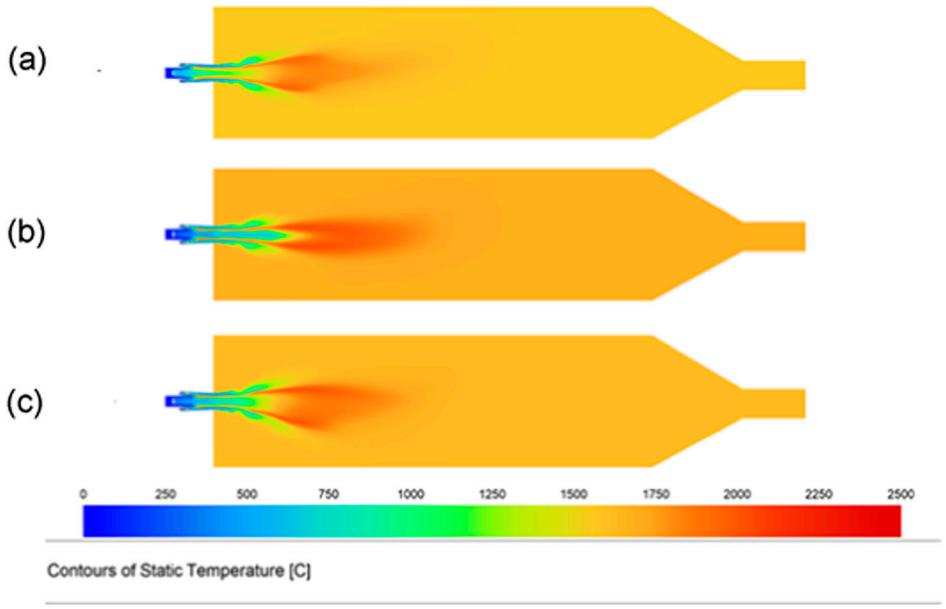

FIGURE 16
CFD model prediction of gas isotherms illustrating jet expansion and quiescent gas atmosphere entrainment around flame region for **(a)** dedicated natural gas firing **(b)** dedicated hydrogen firing and **(c)** cofiring 50% natural gas with 50% hydrogen, all with 10% excess air.

entrainment and recirculation of gases from the chamber promotes complete mixing of the combustion products and ingress air, thereby cooling the gases. The proportion of ingress air to total air increased with hydrogen composition of the fuel, owing to the smaller volume flow of combustion air required through the burner leading to the additional air having a greater effect at elevated proportions of hydrogen cofiring.

Equilibrium temperatures of the gas volume and chamber surfaces became established by the reflection, absorption and re-radiation of energy between surfaces, alongside the recirculation and mixing of gases within the chamber and led to the development of a uniform temperature region within the chamber, extending throughout the central 2.5 m of the furnace length and 600 mm of the width. This equalisation of heat exchange provided a volume from which gas temperatures, chamber temperatures, gas compositions and radiative heat exchange could be considered representative of the fully mixed gases in the chamber, apart from the effects locally to the burner and exhaust flue. The uniformity of chamber conditions enabled evaluation of the effects upon the heating chamber and process of different conditions, such as varying fuel composition, with a reduced set of sample positions.

5.2 Gas temperature distribution

Gas temperature transects through the region of combusting gases demonstrated that the maximum gas temperature occurred on the burner centreline for dedicated natural gas firing and cofiring with low proportions of hydrogen in the fuel, whilst increased hydrogen proportions led to the lateral offset of the peak temperature, as illustrated by Figure 13. This phenomenon was repeatable for different lower and higher proportions of hydrogen in the fuel composition but the underlying causes would need to be verified by comprehensive and thorough experimental and CFD modelling investigations.

The geometry of the burner inlet manifolds resulted in swirl of the gas and air passing through the burner quarl, as demonstrated by the CFD model predictions, illustrated in Figures 17a,b. This may have caused the lateral displacement of the flame peak observed when firing with fuel having higher hydrogen composition. The appearance of this asymmetry at higher hydrogen fuel compositions raises the potential of fluid dynamic effects that would also need to be proven experimentally and analysed using CFD modelling.

The gas temperature profile demonstrated that substantially uniform conditions were achieved across the chamber width and along the length, once combustion had completed and the atmosphere mixing was sufficient to be a quiescent atmosphere. Quiescent and uniform conditions that would not detrimentally affect the gas temperature measurements enabled centreline only measurements to be used as representative of conditions throughout the chamber, for example, for comparison of changes in parameters whilst the proportions of hydrogen and natural gas in the fuel were changed.

The lower and more variable gas temperatures observed with increased hydrogen composition of the fuel were caused by cooling of the furnace atmosphere gases, incurred due to the additional excess air introduced from the purge flow and sub-optimal control at low flow rates. Whilst this indirect effect would be eliminated by improved flow control and reduction of purge flow rates, it also highlights the need for detailed specification of operating condition uniformity and control tolerance requirements for industrial processes. Ensuring optimal design of heating plants to achieve process specifications ideally uses CFD modelling of the thermo-fluid dynamics and interactions with the solid structure to identify and test potential improvements.

The control of hydrogen firing and co-firing processes will need further development and optimisation to achieve suitable tolerance around temperature set points with variable fuel compositions. This may present an ideal case for the development and application of non-linear control systems to achieve this across a broader (and potentially variable) range of operating conditions, particularly with scarcity of hydrogen supplies as more processes become decarbonised and demand exceeds production capacity further. Fuel fungibility from co-firing hydrogen with natural gas in any composition without compromising the processes will afford high temperature and energy-intensive manufacturing industries the capability to vary and optimise fuel mixtures, based upon overall efficiency, fuel availability and costs in real time.

5.3 Gas species distribution

The near burner measurements for 100% natural gas firing and cofiring hydrogen up to 50% by thermal input demonstrated CO and CH_4 peaks around the burner centreline, as would be expected. The CO and CH_4 peaks were displaced from the centreline to approximately 50–100 mm off-centre when cofired with 50% or higher proportions of hydrogen, illustrated in Figures 19, 21 for gas species. This behaviour suggested that the geometry of gas and air inlets to the burner, flame development and ingress air combined to cause flame eccentricity, rather than the wholly axial behaviour observed at other conditions and illustrated in Figures 16–18.

Investigations would need to be undertaken over the range of hydrogen and natural gas fuel mixtures for which this lateral shift occurred but with increased granularity of the fuel mixture ratio to identify the range over which the transition occurred and whether there was a measurable progression with composition or point change.

The high oxygen concentration measured was caused by a combination of the following effects:

- The air to fuel ratio was sub-optimal at low flow rate set points, resulting in higher excess air in the chamber and increasing the excess oxygen concentration by approximately 2 percentage points
- The viewing window air purge supply provided extraneous air into the chamber that increased the excess oxygen within the chamber by approximately 3-4 percentage points

The inaccuracy of flow control was demonstrably a consequence of the flow rate actuation not being optimally configured for lower firing rates and the dilution of the atmosphere by purge air supplies mixing into the flame by mass entrainment/recirculation into the flame region. The control limitations and extraneous air flows introduced uncertainties between the flow rates measured, the set points and the volume of air entrained into the flame, thereby affecting combustion species concentrations within the flame envelope and the fully mixed combustion products atmosphere. The effects of sub-optimal control actuation occurring at turn-down is known to affect manufacturing processes and may be mitigated by applying improved control strategies. The flow rate actuation uncertainties could be improved by applying non-linear characteristics to the electronic control loop governing valve operation and potentially by improved alignment of the actuator and controller ranges with the operating ranges of the furnace, thereby affording better achievement of set points. This step would afford improved tolerance of the response characteristics across a wider range of firing rates, which has been demonstrated successfully on industrial furnaces (Martineau et al., 2002; Martineau et al., 2004).

Correcting the excess air to 3% (dry) free oxygen stipulated for comparing NOx emissions for different excess air firing conditions of hydrocarbon fuels was determined to represent approximate equivalence of the total mass of NOx emissions between different fuel compositions. The correction formula applicable to hydrocarbon fuels causes higher specific NOx emissions to be evaluated than would be valid when firing hydrogen, owing to the increased volumetric proportion of water vapour in the combustion products having a disproportionate effect upon conversion to dry basis. Applying the hydrocarbon correction for excess oxygen to the NOx measurement for hydrogen co-firing and dedicated firing would therefore have been invalid and misleading.

The increased generation of NOx and lower concentrations of CO and CO_2 with increasing proportion of hydrogen in the fuel were demonstrated in the mean values of gas species measured in the fully mixed gas atmosphere. High excess oxygen concentrations were caused by the unaccounted air, as discussed, which also reduced chamber temperatures with fuel mixture variation at steady-state firing rates and static nominal air to fuel ratio set points.

These outcomes would be expected from increased flame temperatures that promote the formation of thermal NOx (Ilbas et al., 2005; Pan et al., 2023) and the elimination of carbon from the fuel mixture. The NOx concentration measured in the fully mixed gases when cofired and fired with 100% hydrogen were approximately double compared to dedicated natural gas firing. Increased NOx would be expected, albeit the concentrations arising were low. The increased magnitude of NOx concentration relative to natural gas firing was comparable to previous measurements on furnaces fired with hydrogen without any mitigation measures (Ilbas et al., 2005). The furnace temperatures used for these tests were relatively moderate which may have suppressed the formation of NOx that would have been higher at elevated temperatures (Pan et al., 2023).

The CFD predictions demonstrated similar flame ‘shapes’ to those apparent from the gas temperature and species distributions measured, that is, peak gas temperatures occurring eccentrically for the cases co-firing higher proportions of hydrogen in the fuel composition. The model outcomes also demonstrated that the dedicated natural gas and hydrogen firing cases had concentric jets issuing from the combustion region, with swirl imposed into the flow fields that caused turbulence. These flame ‘shapes’ arose principally as transient distributions that were not necessarily consistent between specific cases with the model representing temporal snapshots of what is expected to be dynamic behaviour in the combustion region.

Further and more detailed experimental measurement and CFD modelling investigations will be needed to understand and mitigate the causes of flame asymmetry and changes with different fuel mixtures. Understanding the effects of fuel switching on the operation of specific manufacturer’s burners will become important for applying CFD modelling to represent full-scale manufacturing plants within engineering design studies.

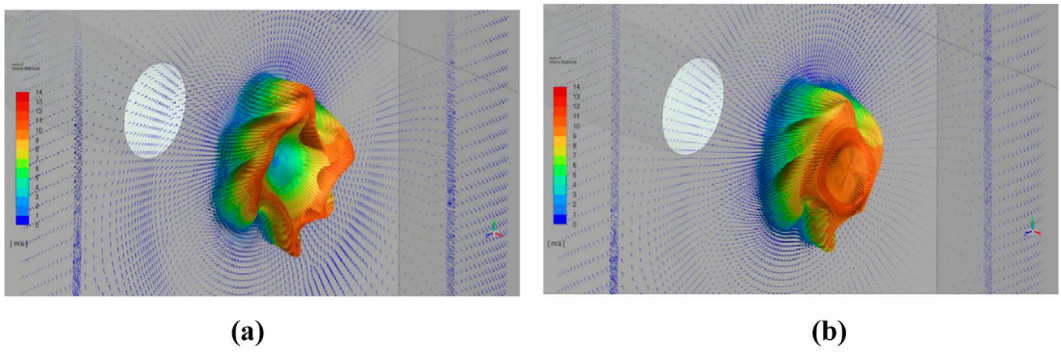

FIGURE 17
CFD prediction of combustion region fluid dynamics local to the burner quarl – the velocity vectors, coloured by velocity magnitude (m/s) – **(a)** with dedicated natural gas firing and 10% excess air, demonstrating entrainment from the adjacent atmosphere and swirl of the jet and **(b)** dedicated hydrogen firing and 10% excess air, demonstrating entrainment from the adjacent atmosphere and swirl of the jet.

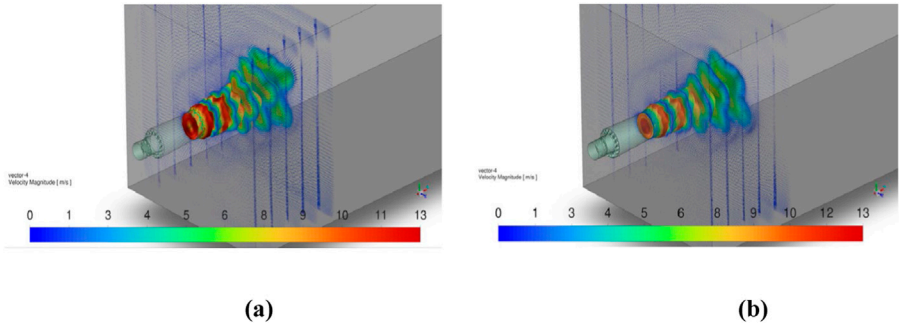

FIGURE 18
(a) Projection of combusting gases into the chamber, illustrating entrainment and expansion of jet, shown via velocity vectors, coloured by velocity magnitude (m/s), for dedicated natural gas firing and 10% excess air and **(b)** Projection of combusting gases into the chamber, illustrating entrainment and expansion of jet, illustrating entrainment and expansion of the jet, shown via velocity vectors, coloured by velocity magnitude (m/s), for dedicated hydrogen firing and 10% excess air.

5.4 Measurement uncertainties

The simple measurement uncertainties associated with each probe point have been estimated, based upon the data acquired from different positions in the chamber and known uncertainty estimates for each probe, as presented in Table 3. These uncertainty estimates are independent for each parameter, for example, gas temperature, radiant heat flux and species distributions are not considered correlated, other than arising from the same gas flows and recirculation patterns. The uncertainty from one measurement has not been propagated to other parameters or an overall uncertainty, owing to this independence of measurements, that enables inference that the simple measurement uncertainties evaluated represented the overall uncertainty.

These uncertainties represent the maximum estimated values and defined that there may be variation occurring within these tolerances around the mean values (central tendency) of parameters reported. The conclusions drawn are not undermined by having uncertainty tolerances around the mean values but do then have lower statistical certainty attached.

6 Conclusions and recommendations

Dedicated firing of hydrogen and co-firing hydrogen with natural gas has been demonstrated to provide equivalent heating conditions to dedicated natural gas use for moderate to high temperature processes. Operating temperatures in the range of 800–900 °C, as used herein, are typical of processes used in primary materials manufacturing, such as metals, glass, ceramics and minerals. These types of processes are particularly prevalent within the energy-intensive foundation industries, which have hard-to-abate CO_2 emissions and therefore direct switching to decarbonised fuels afford a capability to operate without requiring post-combustion carbon capture processes. This investigation enabled evaluation of the suitability of hydrogen as an interoperable fuel to substitute, either partially or wholly, for natural gas through extensive experimental determinations of heat transfer, gas temperatures and gas composition for a range of operational variations, complemented with CFD modelling for equivalent process conditions.

TABLE 3 Uncertainty estimates for parameter measurements on pilot scale furnace.

Parameter	Units	Typical K = 1σ uncertainty %
Gas temperature	°C	2 (fully mixed gas) 6 (combustion region)
Gas concentration	vol% (mol%) ppm	10 10
Radiative heat flux density	kW/m^2	5.7

The total radiation heat transfer achieved between solid surfaces within the heating chamber when fired solely with hydrogen or co-fired with hydrogen and natural gas was comparable to the heat flux achieved when firing natural gas at the same furnace operating conditions. The heat exchange within the pilot process chamber operated at moderate to high temperatures was determined principally by the chamber operating temperature. The air to fuel ratio achieved, alongside the thermal input rate (burner firing rate) and exhaust gas temperature and flow rate affected the steady-state temperature.

There was no evidence of a relationship between the composition of fuel combusted and heat transfer achieved within the chamber volume. The volume of a process chamber and its operating temperature are known to affect the total radiant heat transfer, therefore temperature uniformity is achieved by equalising the radiation heat exchange between the solid surfaces and product within a chamber.

Gas temperatures were measured to have achieved uniform distribution within 10% of the mean gas temperature throughout the centremost volume of the chamber, extending for approximately 2/3 of the furnace length and width. The regions outside of this uniform volume of the chamber were local to the flame envelope and exhaust flue entry. The fully mixed gas temperature and temperature uniformity measured were independent of the fuel mixture supplied into the chamber. CFD modelling of the gas temperature and species distributions throughout the chamber volume demonstrated similar uniformity away from the burner and exhaust flue.

Complete mixing of the products of combustion was achieved after the first metre of the chamber length, that is, immediately after the combustion region and led to the distribution of gas temperatures and fluid flow fields to be uniform throughout 2/3 of the volume. The chamber surface temperatures and radiant heat exchange therefore also achieved uniformity throughout this region and enabled reduced sample positions to represent the fully mixed conditions. Mixing of the gas atmosphere was driven by momentum of the combusting mixture from the burner issuing into the chamber volume and entrainment of combustion products into the flame region creating recirculation of the gases and dilution of the combusting mixture.

Additional experimental investigation and CFD modelling is required to verify the causes of the flame shape asymmetry at specific conditions observed in measurements and initial modelling. The fully mixed atmosphere was not affected by the flame shapes observed, so this step will help users and process designers to understand how hydrogen firing might affect the processes. Ultimately however, this effect will have little expected impact upon the productivity or outcome of the process because the fully mixed gases were observed to be uniform within the useful heating region of the chamber.

As demonstrated herein, hydrogen may be used as a fuel to replace up to 100% of the energy supplied by natural gas within industrial combustion systems that use diffusion flame/nozzle mix burners. This type of burner has typically been fitted to process furnaces, kilns and thermal oxidisers that have combustion product atmospheres in contact with the product. Diffusion flame/nozzle mix burners do not incur flashback because of the thermo-fluid dynamics of the combustion zone and mixing of the fuel and air externally to the supply pipelines, thereby not presenting a pathway for a flame front to regress into the supply line.

This investigation provided evidence that co-firing and/or dedicated hydrogen firing could substitute for natural gas in high temperature processes that use nozzle mix burners, supporting the interoperability of decarbonised fuel for switching from fossil-based fuels. High temperature process operators, such as energy-intensive manufacturing industries can vary the ratio of natural gas and hydrogen used for co-firing without affecting the productivity of their processes, provided that the other operating conditions, principally: chamber temperature, excess oxygen concentration, exhaust gas flow rate and temperature set point remain unaltered. This would therefore enable the use of higher proportions of hydrogen when available, but lower levels if there are supply variations or constraints. The expectation that sufficient hydrogen will not become available to operate energy-intensive manufacturing processes wholly on hydrogen and the potential costs incurred acquiring sufficient hydrogen supplies will necessitate fuel fungibility.

It would always be prudent to model a process using CFD to verify the effects of burner and chamber geometries upon combustion product distribution, furnace and gas temperature distribution and heat transfer between solid surfaces and products within a chamber, when changing operating practices. Whilst hydrogen has been demonstrated to be readily interoperable with natural gas, optimisation of manufacturing processes will require the more detailed understanding of the thermo-fluid dynamics and interactions between fluids and surfaces provided by CFD modelling to be investigated.

Data availability statement

The raw data supporting the conclusions of this article will be made available by the authors, without undue reservation.

Author contributions

AH: Conceptualization, Data curation, Formal Analysis, Funding acquisition, Investigation, Methodology, Project administration, Writing – original draft, Writing – review and editing, Resources. KF: Conceptualization, Data curation, Formal Analysis, Funding acquisition, Investigation, Methodology, Project administration, Writing – original draft, Writing – review and editing, Resources. JS: Conceptualization, Formal Analysis, Investigation, Methodology, Writing – original draft, Writing – review and editing. AG: Formal Analysis, Investigation, Methodology, Writing – review and editing, Writing – original draft. JH: Writing – original draft, Writing – review and editing, Formal Analysis, Investigation, Methodology. MP: Conceptualization, Supervision, Funding acquisition, Resources, Writing – review and editing.

Funding

The author(s) declared that financial support was received for this work and/or its publication. The authors acknowledge the financial support afforded by the UKRI Industrial Decarbonisation Research and Innovation Centre (IDRIC), grant number EP/V027050/1, flexible fund under project FF 4-02.

Acknowledgements

The authors acknowledge the assistance of technical and operations team colleagues: D Gains, S Allen, T Cathcart, A Delorenzi, A Hemstock and T Gregory and professional staff: F Wells at the University of Sheffield, Energy Innovation Centre who made this investigation successful through their dedication to the success of our work and commitment to a nett zero future. The authors also acknowledge the following companies for letters of support, demonstrating foundation industries' interest in the outcome of this project: NSG Pilkington Glass Limited, Breedon Group Limited, British Steel Limited, Siemens plc Industrial Automation and Digital Industries Division and Tata Steel United Kingdom Limited.

Conflict of interest

The author(s) declared that this work was conducted in the absence of any commercial or financial relationships that could be construed as a potential conflict of interest.

Generative AI statement

The author(s) declared that generative AI was not used in the creation of this manuscript.

Any alternative text (alt text) provided alongside figures in this article has been generated by Frontiers with the support of artificial intelligence and reasonable efforts have been made to ensure accuracy, including review by the authors wherever possible. If you identify any issues, please contact us.

Publisher's note

References

Ceriello, G., Sorrentino, G., Cavaliere, A., de Joannon, M., and Ragucci, R. (2021). Mini-review: Heat transfer mechanisms in MILD combustion systems. *Front. Mech. Eng.* 7, 505923. doi:10.3389/fmech.2021.505923

Demuynck, J., De Paepe, M., Huisseune, H., Sierens, R., Vancoillie, J., and Verhelst, S. (2011). On the applicability of empirical heat transfer models for hydrogen combustion engines. *Int. J. Hydrogen Energy* 36 (1), 975–984. doi:10.1016/j.ijhydene.2010.10.059

Forstall, W., Jr, and Shapiro, A. H. (1950). Momentum and mass transfer in coaxial gas jets. *ASME J. Appl. Mech.* 17 (4), 399–408. doi:10.1115/1.4010167

Griffin, P. W., and Hammond, G. P. (2019). Industrial energy use and carbon emissions reduction in the iron and steel sector: a UK perspective. *Appl. Energy* 249 (May), 109–125. doi:10.1016/j.apenergy.2019.04.148

Ilbas, M., Yılmaz, I., Nejat Veziroglu, T., and Kaplan, Y. (2005). Hydrogen as burner fuel: modelling of hydrogen-hydrocarbon composite fuel combustion and NOx formation in a small burner. *Int. J. Energy Res.* 29, 973–990. doi:10.1002/er.1104

Khan, Y. U., Lawson, D. A., and Tucker, R. J. (1997). Simple models of spectral radiative properties of carbon dioxide. *Int. J. Mass Heat. Trans.* 40 (15), 3581–3593. doi:10.1016/s0017-9310(96)00390-0

Kounalakis, M. E., Sivathanu, Y. R., and Faeth, G. M. (1991). Infrared radiation statistics of nonluminous turbulent diffusion flames. *J. Heat. Transf. Trans. ASME* 113, 437–445. doi:10.1115/1.2910580

Leckner, B. (1972). Spectral and total emissivity of water vapour and carbon dioxide. *Combust. Flame* 19, pp33–pp48. doi:10.1016/s0010-2180(72)80084-1

Leicher, J., Schaffert, J., Carpentier, S., Albus, R., and Görner, K. (2020). "Impact of hydrogen admixture on combustion processes," in *Horizon Europe project THyGA public report*.

Liu, Z., Xiong, Y., Yang, N., Ren, L., Liu, Y., Zhang, S., et al. (2023). Comparison of combustion characteristics of MILD model combustor and multi-nozzle array model combustor fueled hydrogen-methane mixtures. *Int. J. Hydrogen Energy* 48, 31802–31812. doi:10.1016/j.ijhydene.2023.04.326

Lopez-Ruiz, G., Blanco, J. M., Peña, A., Romero-Anton, N., and Azkorra-Larrinaga, Z. (2024). CFD study of flameless combustion in a real industrial reheating furnace considering different H2/NG blends as fuel. *Int. J. Hydrogen Energy* 49, 1362–1374. doi:10.1016/j.ijhydene.2023.11.149

Martineau, S., Burnham, K. J., Minihan, J. A., Marcroft, S., Andrews, G., and Heeley, A. (2002). Application of a bilinear pid compensator to an industrial furnace. *IFAC*

Martineau, S., Burnham, K. J., Haas, O. C. L., Andrews, G., and Heeley, G. (2004). Four-term bilinear PID controller applied to an industrial furnace. *Control Eng. Pract.* 12. doi:10.1016/S0967-0661(03)00147-3

Mayr, B., Prieler, R., Demuth, M., and Hochenauer, C. (2017). Comparison between solid body and gas radiation in high temperature furnaces under different oxygen enrichments. *App Therm. Eng.* 127, 679–688. doi:10.1016/j.applthermaleng.2017.08.054

Mayrhofer, M., Koller, M., Seemann, P., Prieler, R., and Hochenauer, C. (2021). Assessment of natural gas/hydrogen blends as an alternative fuel for industrial heat treatment furnaces. *Int. J. Hydrogen Energy* 46 (41), 21672–21686. doi:10.1016/j.ijhydene.2021.03.228

Mayrhofer, M., Koller, M., Seemann, P., Prieler, R., and Hochenauer, C. (2022). MILD combustion of hydrogen and air – an efficient modelling approach in CFD validated by experimental data. *Int. J. Hydrogen Energy* 47 (9), 6349–6364. doi:10.1016/j.ijhydene.2021.11.236

Oh, J., Noh, D., and Ko, C. (2013). The effect of hydrogen addition on the flame behavior of a nonpremixed oxy-methane jet in a lab-scale furnace. *Energy* 62, 362–369. doi:10.1016/j.energy.2013.09.049

Oh, J., and Noh, D. (2015). Flame characteristics of a non-premixed oxy-fuel jet in a lab-scale furnace. *Energy* 81. doi:10.1016/j.energy.2014.12.046

Okafor, E. C., Hayakawa, A., Nagano, Y., and Kitagawa, T. (2014). Effects of hydrogen concentration on premixed laminar flames of hydrogen-methane-air. *Int. J. Hydrogen Energy* 39 (5), 2409–2417. doi:10.1016/j.ijhydene.2013.11.128

Pan, P., Geng, S., Yang, H., Zhang, G., Bian, H., and Liu, Y. (2023). Influence of H2 blending on NOx production in natural gas combustion: mechanism comparison and reaction routes. *Int. J. Hydrogen Energy* 48, 784–797. doi:10.1016/j.ijhydene.2022.09.251

Quinn, T. J. (1967). The calculation of the emissivity of cylindrical cavities giving near black-body radiation. *Br. J. Appl. Phys.* 18, 1105. doi:10.1088/0508-3443/18/11/527

Rhine, J. M., and Tucker, R. J. (1991). *Modelling of gas-fired furnace and boilers and other industrial heating processes, Chapter 10, pp197-211, British Gas plc*. McGraw-Hill Book Company.

Rose, J. W., and Cooper, J. R. (1977). "Technical data on fuel," in The British National Committee, World Energy Conference.

Schmidt, N., Müller, M., Preuster, P., Wasserscheid, P., and Will, S. (2023). Development and characterization of a low-NOx partially premixed hydrogen burner using numerical simulation and flame diagnostics. *Int. J. Hydrogen Energy* 48 (41), 15709–15721. doi:10.1016/j.ijhydene.2023.01.012

Schwartz, S., Daurer, G., Gaber, C., Demuth, M., and Hocehenauer, C. (2024). Experimental investigation of hydrogen enriched natural gas combustion with a focus on nitrogen oxide formation on a semi-industrial scale, *Int. J. Hydrogen Energy* 63, 173–183. doi:10.1016/j.ijhydene.2024.03.190

Shudo, T., and Suzuki, H. (2002). Applicability of heat transfer equations to hydrogen combustion. *JSAE Rev.* 23 (3), 303–308. doi:10.1016/S0389-4304(02)00193-5

Smith, T. F., Shen, Z. F., and Friedman, J. N. (1982). Evaluation of coefficients for the Weighted sum of gray gases model. *Trans. ASME* 104.

Srinivasarao, M., Sorrentino, G., and Mahendra Reddy, V. (2024). Investigation of the interaction of the MILD regime with HiTAC and no-combustion regimes in combustion region diagrams. *Front. Energy Res.* 12, 1503787. doi:10.3389/fenrg.2024.1503787

Tucker, R. J., and Ward, J. (2012). Identifying and quantifying energy savings on fired plant using low-cost modelling techniques. *Appl. Energy* 89, 127–132. doi:10.1016/j.apenergy.2011.01.061

Van Der Drift, A., Tjeng, S. L., Beckers, G. J. J., and Beesteheerde, J. (1996). Low-NOx hydrogen burner. *Int. J. Hydrogen Energy* 21 (6), 445–449. doi:10.1016/0360-3199(95)00105-0

Xu, J., Chen, R., and Meng, H. (2021). WSGG models for radiative heat transfer calculations in hydrogen and hydrogen-mixture flames at various pressures. *Int. J. Hydrogen Energy* 46, 31452–31466. doi:10.1016/j.ijhydene.2021.07.040

Yang, X., Bo, Y., Yang, W., and Zhou, H. (2021). Investigation of heat transfer characteristics of hydrogen combustion process in cylindrical combustors from microscale to mesoscale. *Int. J. Hydrogen Energy* 46, 25893–25907. doi:10.1016/j.ijhydene.2021.05.099

Zhang, X., Ai, Q., and Wang, W. (2023). Effects of gas models on radiative heat transfer in the combustion chamber of a hydrogen gas turbine. *Int. J. Hydrogen Energy* 48 (77), 30144–30155. doi:10.1016/j.ijhydene.2023.04.193

Zhi, Y., Zhang, W., Yang, Q., Li, G., and Chen, H. (2018). Influence analysis of the furnace wall emissivity on heating process. *Infrared Phys. Technol.* 93, 326–344. doi:10.1016/j.infrared.2018.08.009